Available online at www.sciencedirect.com

ScienceDirect

Journal of Magnesium and Alloys 6 (2018) 356–365

www.elsevier.com/locate/jma

Full Length Article

Corrosion protection of AZ91D magnesium alloy by a cerium-molybdenum coating. The effect of citric acid as an additive

I.L. Lehr*, S.B. Saidman

Instituto de Ingeniería Electroquímica y Corrosión (INIEC), Departamento de Ingeniería Química, Universidad Nacional del Sur (UNS), CONICET, Bahía Blanca, Argentina

Received 13 April 2018; received in revised form 3 October 2018; accepted 8 October 2018
Available online 28 November 2018

Abstract

In order to improve the corrosion resistance of AZ91D magnesium alloy, a coating was formed by a potentiostatic technique from a solutions containing $Ce(NO_3)_3$, Na_2MoO_4 and citric acid (H_3Cit). The degree of corrosion protection achieved was evaluated in simulated physiological solution by monitoring the open circuit potential, polarization techniques and electrochemical impedance spectroscopy (EIS). Surface analysis techniques (SEM, EDS, X-ray diffraction and X-ray photoelectron spectroscopy (XPS)) were used for coating characterization. The film is mainly composed by cerium and molybdenum oxides and magnesium oxides and hydroxides. The obtained results show that the corrosion resistance of the coated electrodes has been increased significantly. This improvement in the anticorrosive performance is in part due to the corrosion inhibition properties of H_3Cit.

Keywords: Cerium and molybdenum-based coatings; AZ91D alloy; Citric acid; Anticorrosive properties.

1. Introduction

Magnesium and its alloys are promissory materials for temporary implants due to their interesting combination of engineering properties such as low density, high specific strength and stiffness, excellent machinability and good castability [1,2]. These light-weight materials are biocompatible and biodegradable in physiological environment. Moreover, they have physical and mechanical properties similar to natural bone [3]. However, the major disadvantages of Mg alloys are their poor resistance to corrosion and high chemical reactivity which have hindered a wider use in many applications [4–7].

To improve the corrosion resistance of magnesium alloys several surface treatments have been proposed, such as chemical conversion, anodization, laser and ion beams, PVD (Physical Vapor Deposition) coatings and CVD (Chemical Vapor Deposition), electroless plating and deposition of organic coatings [8–11]. All these surface treatments aim to modify the surface of the alloys without affecting their bulk performance. Some of these methods have been claimed to be able to offer good corrosion protection. Treatments that modify the oxide surfaces are known for their low cost and simplicity of operation. Anodization is one of the most important and effective surface pretreatments for Mg and its alloys. In contrast to other surface treatments for these materials, anodization can produce a relatively thick, hard, adherent and abrasion-resistance film [12].

The use of molybdate in different treatments to protect Mg alloys against corrosion has been the subject of various works [13–15]. Molybdate anion has many advantages, such as low toxicity and high stability in aqueous media [16,17]. In a previous work, we showed that the anodization of the AZ91D magnesium alloy in molybdate solutions applying low potentials allowed obtaining coatings with good anticorrosive performance [18]. The improvement in the corrosion resistance is associated with the presence of molybdenum species in the formed film.

* Corresponding author
E-mail address: ilehr@uns.edu.ar (I.L. Lehr).

https://doi.org/10.1016/j.jma.2018.10.002

On the other hand, the formation of cerium-based coatings on Mg alloys have been intensively studied [19,20]. These coatings increase the corrosion resistance of magnesium biodegradable alloys in simulated physiological media. It is known that the use of H_2O_2 as an additive leads to the formation of a more compact film [21–24]. Wang et al. reported that a cerium coating obtained by a galvanostatic technique showed better corrosion resistance compared to the film formed by open circuit conditions on AZ91D magnesium alloy [25]. Du et al. studied the corrosion resistance of a Mo-Ce conversion coating on AZ91 magnesium alloy and reported an improvement in the corrosion resistance of the alloy after 10 min of immersion in a solution of sodium molybdate and cerium nitrate at 25 °C [13]. We have shown in a previous work that a cerium-based coating prepared from a solution containing $Ce(NO_3)_3$, H_2O_2 and ascorbic acid (HAsc) on AZ91D alloy offered a superior corrosion protection in simulated physiological solution compared with the film formed in the absence of HAsc [26]. The improvement in the anticorrosive properties is associated with the combination of the characteristics of the cerium oxides and the inhibitory effect of the additive.

In the present work, we report the formation of cerium and molybdenum-based coatings on AZ91D magnesium alloy by a potentiostatic technique. The influence of citric acid as an additive in the treatment solution was analysed. Optimal experimental conditions were determinate to obtain films with a good anticorrosive performance in simulated physiological solution.

2. Experimental

The working electrodes were prepared from rods of AZ91D magnesium alloy (composition: 8.978% Al, 0.6172% Zn, 0.2373% Mn, 0.2987% Si, 0.1189% Cu, 0.00256% Ni, 0.0176% Fe, 0.00164% Ca, 0.01154% Zr, remainder Mg). The rods were embedded in a Teflon holder with an exposed area of 0.070 cm^2. Before each experiment, the exposed surfaces were polished to a 1000 grit finish using SiC, then degreased with acetone and washed with triply distilled water. Following this pretreatment, the electrode was immediately transferred to the electrochemical cell. All the potentials were measured against a saturated Ag/AgCl and a platinum sheet was used as a counter electrode. The cell was a 20 cm^3 Metrohm measuring cell.

The electrodes were treated in an electrolyte solution containing cerium nitrate hexahydrate $Ce(NO_3)_3{\cdot}6H2O$ (5–50 mM) and $Na_2MoO_4{\cdot}2H_2O$ (5–20 mM) in a purified nitrogen gas saturated atmosphere. Citric acid (H_3Cit) was used as additive and its concentration was varied between 1 and 30 mM. The temperature employed was 50 °C. All chemicals were reagent grade and solutions were made in twice distilled water.

Electrochemical measurements were done using a potentiostat–galvanostat Autolab PGSTAT 128 N and VoltaLab40 Potentiostat PGZ301. The frequency used for the impedance measurements was changed from 100 kHz to 10 mHz and the signal amplitude was 10 mV. The morphologies of the synthesized coatings were investigated by scanning electron microscopy (dual stage ISI DS 130 SEM), equipped with energy dispersive spectrometry (EDAX 9600). X-ray diffraction analysis was carried out using a Rigaku X-ray diffractometer (model Dmax III-C) with Cu Kα radiation and a graphite monochromator. In order to examine the chemical composition of coatings X-ray photoelectron spectroscopy (XPS) was performed in a Specs setup operating. The XPS analysis chamber is equipped with a dual anode (Al/Mg) X-ray source and a 150 mm hemispherical electron energy analyzer (PHOIBOS). The analyzer operated in fixed analyzer transmission (FAT) mode with pass energy of 30 eV. The energies of all spectra were referenced to the C 1 s peak at 285.0 eV. All the XPS spectra were deconvoluted using the CASA XPS software with a Gaussian-Lorentzian mix function.

Film adhesion was tested measuring the force necessary to peel-off the film using a Scotch® MagicTM double coated Tape 810 (3 M) and a Mecmesin basic force gauge (BFG 50 N).

The corrosion performance was investigated in Ringer solution at 37 °C by a potentiodynamic method, by the variation of the open circuit potential (OCP) as a function of time and by electrochemical impedance spectroscopy (EIS). The electrodes were allowed to equilibrate at the fixed voltage before the ac measurements. The composition of Ringer solution is (per 1 L) 8.60 g NaCl, 0.30 g KCl and 0.32 g $CaCl_2.2H_2O$.

The Tafel tests were carried out by polarising from cathodic to anodic potentials with respect to the open circuit potential at 0.001 Vs^{-1} in Ringer solution. Estimation of corrosion parameters was realized by the Tafel extrapolation method. The extrapolation of anodic and cathodic lines for charge transfer controlled reactions gives the corrosion current density (i_{corr}) at the corrosion potential (E_{corr}). All experiments were conducted approximately 30 min after immersion in the Ringer solution. Electrochemical impedance spectra were obtained at the open circuit potential (OCP) in the frequency range from 100 kHz to 100 mHz, and the signal amplitude was 10 mV. Furthermore, the EIS data were analyzed and modeled into equivalent electrical circuits (EEC) with Z-View software. All experiments were conducted after the steady-state E_{corr} was attained. Each set of experiments was repeated two to four times to ensure reproducibility.

3. Results

3.1. Evaluation of the anticorrosive properties of the coatings

Electrolyte solution composition and applied potential were varied to establish the best conditions for coating formation. First, the alloy was treated in a $Ce(NO_3)_3$ solution under potentiostatic control or under open circuit potential (OCP) conditions. It was not possible to form a coating after immersion of the substrate under OCP conditions in 30 mM $Ce(NO_3)_3$, pH 4.0. On the other hand, when the $Ce(NO_3)_3$ concentration

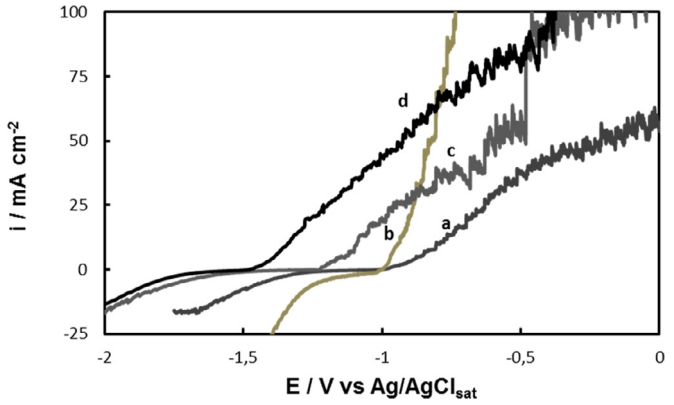

Fig. 1. The polarization behavior in Ringer solution of Ce-coat formed on AZ91D magnesium alloy in 30 mM $Ce(NO_3)_3$ at: (a) −0.30 V, (b) −0.60 V and (c) 0.30 V. For comparison the polarization curve of uncoated AZ91D alloy was also included (d). The scan rate was 0.001 Vs^{-1}.

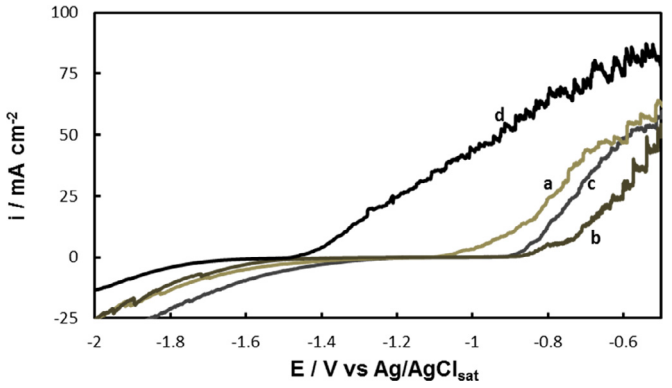

Fig. 2. The polarization behavior in Ringer solution of Ce-Mo-coat formed on AZ91D magnesium alloy formed at −0.30 V in 30 mM $Ce(NO_3)_3$ and x mM Na_2MoO_4, with x: (a) 5 mM, (b) 15 mM, (c) 30 mM. For comparison the polarization curve of uncoated AZ91D alloy was also included (d). The scan rate was 0.001 Vs^{-1}.

was below 30 mM the electrode surface was partially covered by a grayish-white film after polarization in the potential range between −0.60 V to 0.60 V during 30 min. A concentration of 30 mM leads to the formation of a Ce coating completely covering the substrate. Therefore, this concentration was selected.

In order to evaluate the influence of the applied potential on the anticorrosive performance of the formed films, polarization measurements were recorded in Ringer solution for the alloy previously polarized at different potentials in 30 mM $Ce(NO_3)_3$ (Fig. 1). For comparison, the polarization curve obtained for the untreated substrate is also presented (Fig. 1, curve d). The anodic polarization curve of bare AZ91D alloy presents a current density increase at approximately −1.50 V, which indicates active dissolution. Significant current oscillations can be observed at more anodic potential values. Pardo et al. suggested that the AZ91D alloy suffer pitting attack immediately after its immersion in the aggressive media [27]. These authors concluded that, contrary to what might be expected, general corrosion attack was the main mechanism of degradation of this alloy due to the fast growth of corrosion products on the material surface. By comparing the polarization curves, it is evident that the coatings provide an improvement in the corrosion resistance (Fig. 1, curves a-c). In all cases, a white insoluble precipitate appeared at the end of the potential scan denoting alloy dissolution. As the Ce layer formed at −0.30 V shows the best anticorrosive performance, this potential was selected for further experiments. For practical purposes the film will be called Ce-coat.

The effect of addition of different concentrations of Na_2MoO_4 to the cerium solution was evaluated. After mixing the two solutions ($Ce(NO_3)_3$ and Na_2MoO_4) a yellow precipitate was observed. Thus, during coating formation the treatment solution was slightly agitated. The reaction between Ce^{3+} and MoO_4^{2-} has been extensively studied by Mittal et al. [28]. They reported the formation of a yellow amorphous precipitate of cerium molybdate $Ce_2O_3.3\ MoO_3$ in the pH range 5.8–6.2. Fig. 2 shows the polarization curves

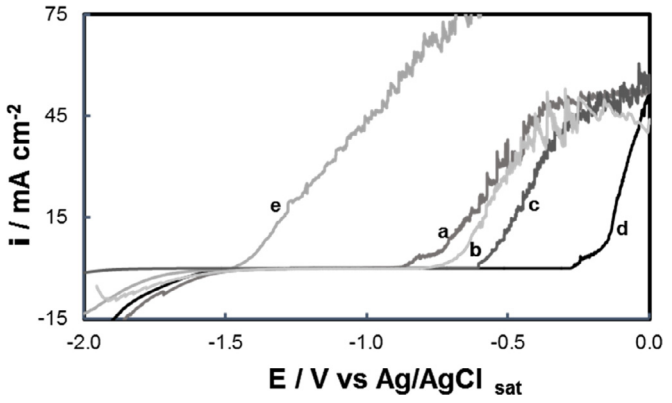

Fig. 3. The polarization behavior in Ringer solution of cerium and molybdate-based films coated AZ91D magnesium alloy formed at −0.30 V during 30 min in 30 mM $Ce(NO_3)_3$, 15 mM Na_2MoO_4 and x mM H_3Cit, with x: (a) 0 mM, (b) 1 mM, (c) 5 mM and (d) 10 mM. For comparison the polarization curve of uncoated AZ91D alloy was also included (e). The scan rate was 0.001 Vs^{-1}.

recorded in Ringer solutions for the coating electrodeposited at −0.30 V during 30 min in 30 mM $Ce(NO_3)_3$ and different concentrations of Na_2MoO_4. The reference curve for the untreated alloy is also given for comparison. The presence of a long passive region for the sample prepared in 30 mM $Ce(NO_3)_3$ and 15 mM Na_2MoO_4 suggests that the formed film exhibits highly protective properties in a Ringer solution (Fig. 2, curve b). Thus, this molybdate concentration was selected and the coating will be called Ce-Mo-coat.

In order to improve the anticorrosive performance of Ce-Mo-coat different concentrations of citric acid (H_3Cit) were added to the treatment solution. Fig. 3 shows the polarization curves for the coatings formed from a solution containing 30 mM $Ce(NO_3)_3$, 15 mM Na_2MoO_4 and different H_3Cit concentrations. For comparison the anodic polarization curve obtained for Ce-Mo-coat was also included. A significant improvement in the corrosion performance was evidenced by the presence of the coatings modified with H_3Cit. At the end of the potentiostatic procedure a yellowish-white film was

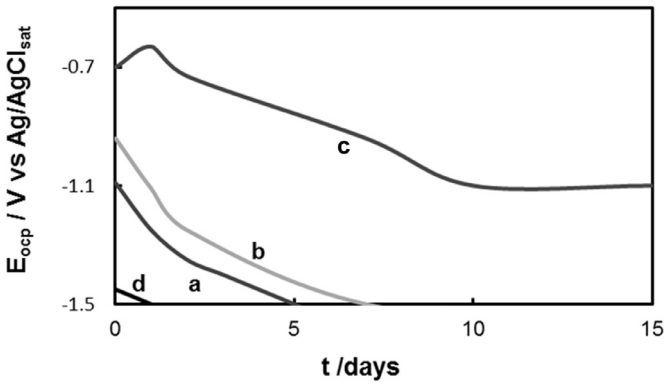

Fig. 4. Time dependence of the OCP in Ringer solution for: (a) Ce-coat, (b) Ce-Mo-coat, (c) Ce-Mo/H_3Cit-coat and (d) uncoated AZ91D magnesium alloy.

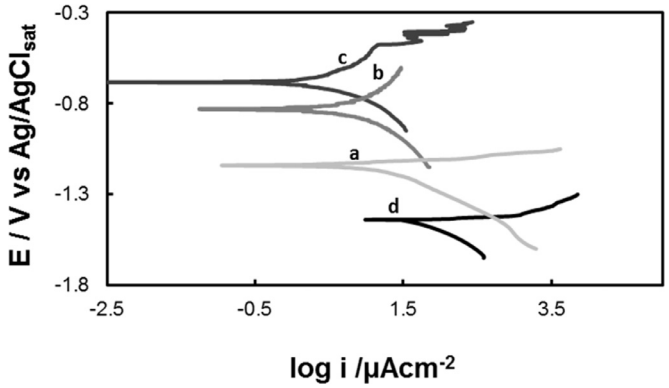

Fig. 5. Tafel curves obtained in Ringer solution for: (a) Ce-coat, (b) Ce-Mo-coat, (c) Ce-Mo/H_3Cit-coat and (d) uncoated AZ91D magnesium alloy. The scan rate was 0.001 Vs^{-1}.

observed by the naked eyes for all coatings. The resulting curves show that 10 mM is the optimal H_3Cit concentration (Fig. 3, curve d). The coating generated at −0.30 V in a solution containing 30 mM $Ce(NO_3)_3$, 15 mM Na_2MoO_4 and 10 mM H_3Cit pH 3.5 will be called Ce-Mo/H_3Cit-coat.

Open circuit potential monitoring as a function of immersion time is usually employed to estimate the degree of corrosion protection attained after covering the substrate with the coating. Fig. 4 depicts the evolution of the OCP of uncoated AZ91D and coated samples during immersion in Ringer solution at 37 °C. In the case of the uncoated alloy, the OCP decreases rapidly from an initial value of about −1.45 V to a minimum value of about −1.53 V (Fig. 4, curve d). This point would indicate the presence of localized corrosion, and then the decrease in OCP is associated with the spread of corrosion across the AZ91D surface [29]. As soon as the substrate was immersed in Ringer solution, the surface was corroded and hydrogen bubbles evolution appeared. After 3–4 h, precipitate of white corrosion products can be observed at the bottom of the electrochemical cell. A similar behavior is observed for the Ce-coat and Ce-Mo-coat although the initial value is more noble than that of the uncoated sample (Fig. 4, curves a and b). For the Ce-Mo/H_3Cit-coat, the change of OCP can be divided into three stages (Fig. 4, curve c). In the first stage, a potential increase was observed within the first 24 h of immersion, probably associated with the deposition of magnesium or aluminum oxides or hydroxides [29]. Then the OCP decreases slowly during 10 days until reaching a steady state at −1.10 V. Thus, the registered OCP values for this coating are more noble than those for the other films evaluated. In addition, a white precipitate was not observed for the Ce-Mo/H_3Cit-coat after testing for 15 days in Ringer solution.

The concentration of Mg released from the samples after immersion in Ringer solution was measured. In the case of the uncoated alloy, the quantity of Mg released was 3.90 mg/L while a value of 1.80 mg/L was obtained for the Ce-Mo-coat. A higher decrease in the quantity of Mg released (0.67 mg/L) was determined when the substrate was coated with the Ce-Mo/H_3Cit-coat. These results confirm the better anticorrosive efficiency of Ce-Mo/H_3Cit-coat even after a long exposure time.

Table 1
I. L. Lehr, S. B. Saidman.

Coating	Adherence force/ N
Ce-coat	23.8
Ce-Mo-coat	32.1
Ce-Mo/H_3Cit-coat	45.3

Fig. 5 compare the Tafel plots for uncoated and coated AZ91D alloy. Table 2 reports values related to the estimation of the corrosion parameters (E_{corr}, cathodic (B_c) and anodic (B_a) Tafel slopes and corrosion current (i_{corr})) for all coatings studied. For all the treated samples, the corrosion potential is higher compared to the one for the untreated alloy. The corrosion potential value increased from −1.095 V for Ce-coat to −0.70 V for Ce-Mo/H_3Cit-coat. The i_{corr} value for Ce-Mo-coat was two orders of magnitude lower than that for uncoated AZ91D alloy. A significant improvement in the corrosion performance is observed for Ce-Mo/H_3Cit-coat, which shows the lowest i_{corr} among all of the samples, by about three orders lower than that of the uncoated substrate. Du et al. reported an improvement in the corrosion properties of AZ91 after 10 min of immersion in a solution composed of sodium molybdate (3–4 g/L) and cerium nitrate (8–10 g/L) at 25 °C [13]. The authors informed that the corrosion potential increased by approximately 90 mV and the corrosion current density was decreased by approximately two orders of magnitude compared with the bare AZ91 magnesium alloy. Then, the potentiostatic deposition of the coating in the presence of H_3Cit as an additive significantly improves the corrosion resistance of AZ91D alloy.

The impedance spectra recorded for the AZ91D alloy without any treatment and after different treatments are shown in Fig. 6. The bare AZ91D magnesium substrate spectrum was characterized by a well-defined capacitive loop in the high-frequency range, which represents the interface reaction between the electrolytic solution and the substrate. An inductance behavior in the low frequency region is displayed which may be related to a change of the surface state due

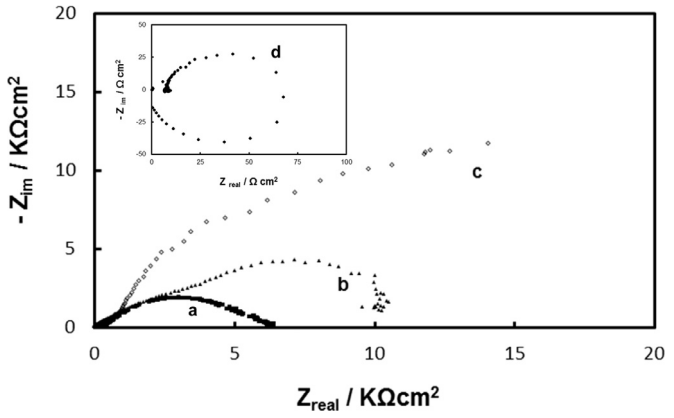

Fig. 6. Nyquist plots of the impedance spectra obtained at the open circuit potential in Ringer solution for: (a) Ce-coat, (b) Ce-Mo-coat and (c) Ce-Mo/H_3Cit-coat. For comparison, the Nyquist plot for uncoated AZ91D alloy after 5 min of immersion was presented (curve d, small insert).

Table 2
I. L. Lehr, S. B. Saidman.

	E_{corr} / V	i_{corr} / mAcm^2	B_a / V	B_c / V
AZ91D	− 1.501 ± 0.050	0.1050 ± 0.0050	0.045	−0.293
Ce-coat	− 1.095 ± 0.050	0.0150 ± 0.0050	0.035	−0.183
Ce-Mo-coat	− 0.785 ± 0.020	0.0090 ± 0.0005	0.418	−0.312
Ce-Mo/H_3Cit-coat	− 0.637 ± 0.020	0.0020 ± 0.0001	0.176	−0.123

to the breakdown of the surface coating in Ringer solution [30] or to adsorbed/desorbed of corrosion products on the sample [31]. The impedance diagrams for the treated samples exhibit two capacitive loops in the high and low frequency ranges. It is important to note that the inductive response was not observed for the coated samples. It is well known that the bigger the diameter of the semicircle the better the corrosion resistance of the sample [32]. In this way, the responses for the coated samples show larger semicircles as compared with uncoated samples, confirming that all coatings improve the corrosion resistance of AZ91D alloy in Ringer solution. According to previous studies [18,26], the capacitive loops for the coated samples in the high frequency range correspond to the charge transfer resistance on the substrate surface (R_{ct}) and coating capacitance (C_c). The low frequency capacitive loop is attributed to the corrosion product layer, the oxide film and the coating on the surface of metal substrate [33]. In summary, it is clear that the presence of Ce-Mo/H_3Cit-coat provides a superior anticorrosive performance for magnesium alloy.

The performance of the Ce-Mo/H_3Cit-coat at different immersion times in Ringer solution was analyzed by Nyquist plots (Fig. 7A). As can be observed, the diameter of capacitive loop decreases gradually with increasing time, indicating that the anticorrosion performance of the coating is reduced with time. However, after 15 days of immersion the total impedance response is still much greater than that obtained for the bare substrate. This result corroborates that the Ce-Mo/H_3Cit-coat can effectively improve the corrosion resistance of the alloy.

To estimate the corrosion performance, experimental impedance spectra of Ce-Mo/H_3Cit-coat at different immersion times in Ringer solution were fitted using equivalent circuits (Fig. 7A). The equivalente circuit described in Fig. 7B is usually utilized to fit EIS data from conversion coating formed on Mg alloys [15]. The fitting resuls of impedance spectra are listed in Table 3. The equivalent circuits make use of a constant phase elements (CPE) as a substitute for a capacitor. The model simulates the experimental data well, considering that the errors of fitting are lower than 5% for all the parameters. In the equivalent circuit proposed for the coating R_s represents the resistance of the solution. R_1 and CPE_1 represent, respectively, the pore resistance and the capacitance of the coating. CPE_2 and R_2 are related to the interface between coating and substrate.

In order to evaluate the corrosion resistance, the values of R_2 are the most important to analyze. From the fitted values, it can be observed a slow decrease in R_2 values with time. This result may be associated with the progressive dissolution of the Ce-Mo/H_3Cit-coat during 15 days of immersion in Ringer solution. Also, it can be noticed that the fitted values of the capacitive components in the circuit remained nearly constant with immersion time.

3.2. Coatings characterization

SEM images of the Ce-Mo-coat and Ce-Mo/H_3Cit-coat were presented in Fig. 8. The morphology of Ce-Mo-coat is of crack-mud structure (Fig. 8A). The cracks may be due to the dehydration of the surface film after the treatment [34]. In the same way, Hamalaoui et al. proposed that the cracked area is associated with the formation of gas bubbles on the substrate, with a dehydration process or also with shearing stresses between the alloys and the coating formed [35]. As shown in Fig. 8B a smooth, compact and uniform coating with tiny cracks was observed for Ce-Mo/H_3Cit-coat. The EDS results confirm the presence of Ce and Mo in both coating studied (Fig. 9).

Fig. 10 shows the XRD patterns of the uncoated AZ91D alloy and coated samples. By comparing the XRD patterns

Table 3
I. L. Lehr, S. B. Saidman.

	Immersion time	Rs (Ω.cm^2)	R_1 (Ω.cm^2)	R_2 (Ω.cm^2)	CPE_1 (F.cm^{-2})	n	CPE_2 (F.cm^{-2})	n
Ce-Mo/H_3Cit-coat	2 h	21.17	2289	34,993	2.56E-5	0.59	5.81E-7	0.96
	1 day	21.2	2200	7635	2.73E-5	0.59	5.81E-7	0.96
	7 days	20.9	2100	3950	2.64E-5	0.59	5.82E-7	0.95
	15 days	21.1	1980	3325	2.52E-5	0.59	5.78E-7	0.96

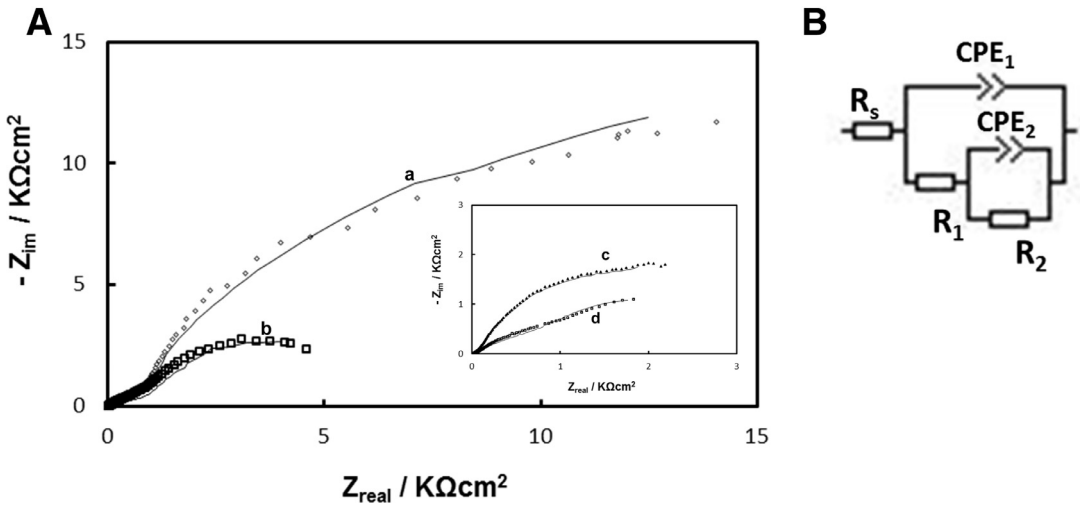

Fig. 7. (A) Nyquist plots of the impedance spectra obtained at the open circuit potential in Ringer solution for Ce-Mo/H_3Cit-coat after different immersion times: (a) 5 min, (b) 24 h, (c) 7 days and (d) 15 days. (○) experimental data; (-) fitted data. (B) Equivalent circuit used for fitting experimental EIS data for Ce-Mo/H_3Cit-coat.

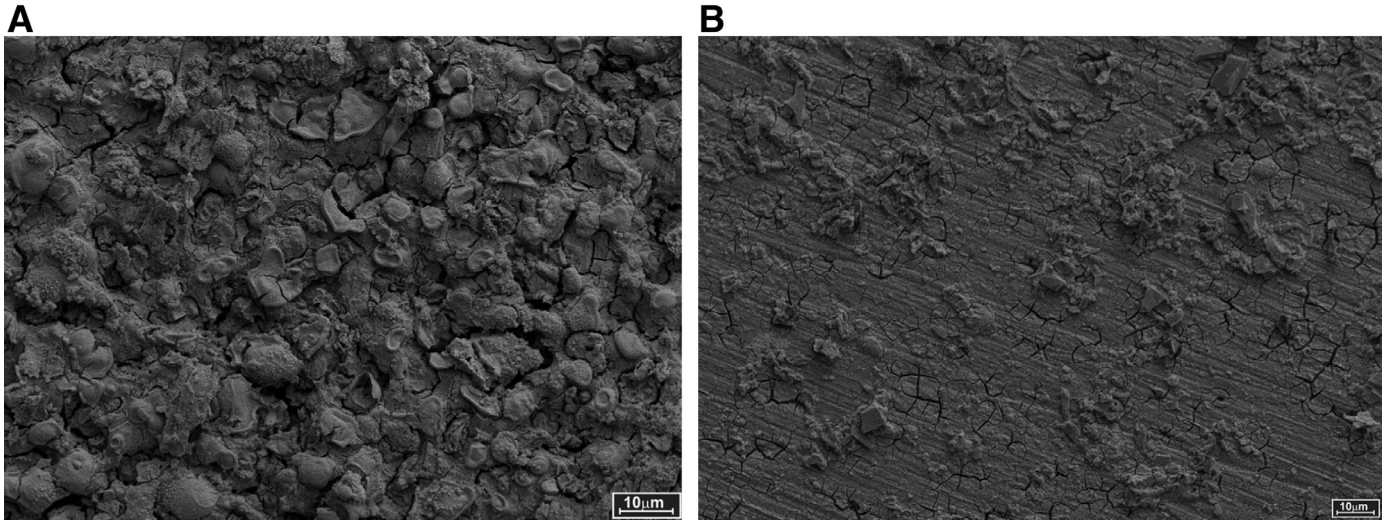

Fig. 8. SEM micrographs of: (A) Ce-Mo-coat and (B) Ce-Mo/H_3Cit-coat.

we can conclude that the coatings are composed of CeO_2, Ce_2O_3, MoO_2, MoO_3 and $Mg(OH)_2$ [13,18,26].

XPS is usually employed to identify the specific electron binding energies of elements at the surface of conversion coating and the main reacting products. Fig. 11A shows the survey spectra of the Ce-Mo/H_3Cit-coat obtained by XPS. Mg, O, Al, Ce and Mo were detected as the major elements. A more detailed XPS analysis of specific electron binding energies of elements was illustrated in Fig. 11B-E. According to the data previously reported [13,18,26], the XPS peaks of each element should be resulted from the corresponding compounds. Fig. 11B shows the Mg 2p sprectrum and the results indicate that Mg in the coating is present as MgO and $Mg(OH)_2$ [36]. As shown in Fig. 11C the fitted peaks of O 1 s corresponding to metallic oxides [13]. The binding energies at about 899.1 eV and 882.1 eV corresponding to Ce^{4+}, 904.1 eV and 885.1 eV corresponding to Ce^{3+} [13,26] (Fig. 11D). The fitted peaks of Mo3d at about 234.8 eV and 232.5 eV correspond to Mo^{6+} and the peaks at 231.9 and 234.5 eV are attributed to the Mo^{4+}, indicating that the conversion coatings consist of a mixture of MoO_2 and MoO_3 (Fig. 11E). Thus, from the results obtained it could be proposed that CeO_2, Ce_2O_3, MoO_2, MoO_3, MgO and $Mg(OH)_2$ constituted the coating.

The force necessary to peel-off the films is shown in Table 1. The presence of H_3Cit in the treatment solution increases the adhesion of the film. All the coatings can be removed only by mechanical polishing.

4. Discussion

The main cathodic reaction during corrosion of magnesium alloys is the reduction of hydrogen ions. The hydrogen discharge causes an increase of the pH in the interface between the alloy and the electrolyte solution, which promotes the

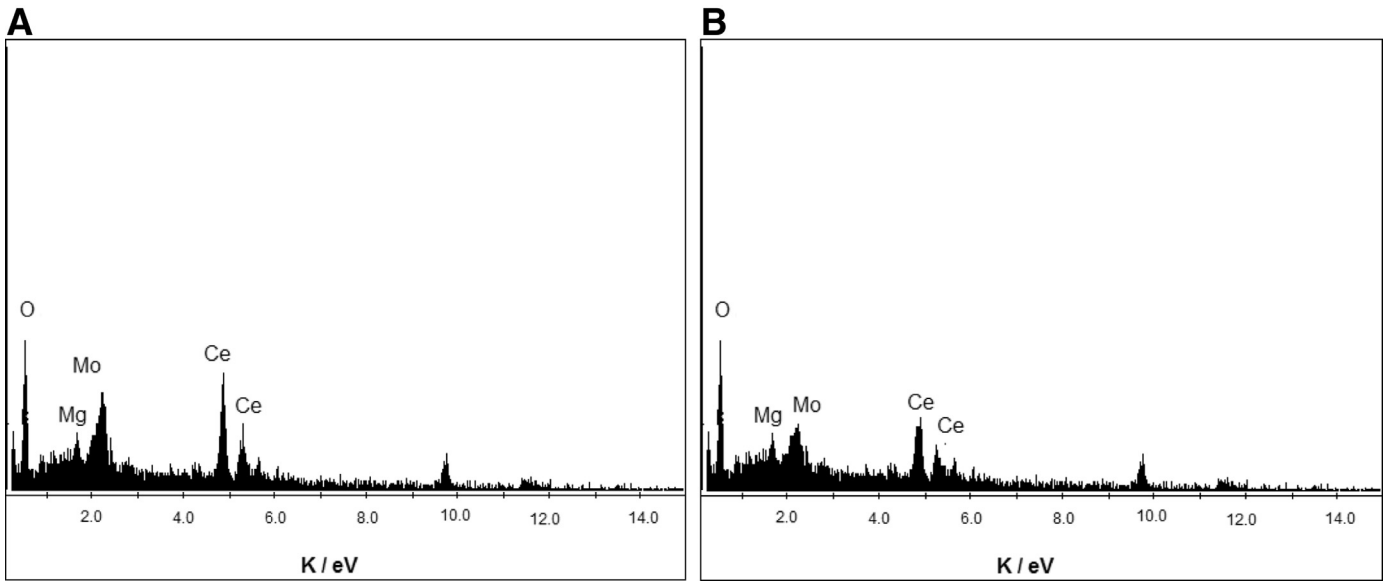

Fig. 9. EDX spectra for: (A) Ce-Mo-coat and (B) Ce-Mo/H_3Cit-coat.

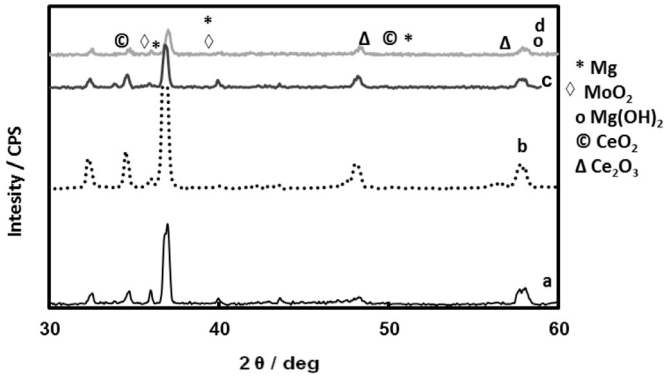

Fig. 10. XRD spectra for: (a) uncoated AZ91D alloy, (b) Ce-coat, (c) Ce-Mo-coat and (d) Ce-Mo/H_3Cit-coat.

reaction of Ce^{3+} and Ce^{4+} species with OH^- to form insoluble salts of $Ce(OH)_3$ and $Ce(OH)_4$ as coating components. It is well known that the inhibiting mechanism for cerium species is related to the formation of these highly insoluble cerium oxides and hydroxides preferentially in active cathodic zones [37,38]. In this way, several authors have proposed that the mechanism for the galvanostatic formation of CeO_2 is based on the local pH increase in the cathodic region [21,39]. It has been reported that electrochemical reactions such as the reduction of water, nitrates or disolved oxygen provided increased pH at the electrode surface [40]. Moreover, it was shown that the valence state of cerium changed from Ce^{3+} to Ce^{4+} at the electrode surface in aerated solutions, resulting in the formation of $Ce(OH)_2{}^{2+}$ species which reacted with electrogenerated OH^- ions to form a precipitate of CeO_2 [41].

On the other hand, molybdenum is well known as a localized corrosion inhibitor when it is present in the electrolyte as Mo(VI) or as an alloying element in iron-based alloys. In the case of Mg alloys, molybdate was used in different treatments to protect these materials against corrosion. It was reported the formation of a molybdate/phosphate conversion coating on Mg-Zn-Y-Zr alloy which improves the corrosion resistance of the substrate [42]. A black protective film was obtained on AZ31 from a molybdate/phosphate/fluorinate aqueous solution [43]. In a previous work we reported the formation of a coating by anodization of AZ91D in molybdate solutions [18]. The improvement in the corrosion resistance of the substrate is associated with the incorporation of molybdenum species in the growing film during anodization treatment.

It is important to consider that the combination of cerium cations and other inhibiting anions can often lead to synergistic corrosion inhibiting properties [44,45]. The inhibiting efficiency of cerium salts combined with molybdate in the corrosion of AA2024 aluminum alloys has been discussed in several works [44–46]. The presence of molybdenum in the coating has been attributed to redox properties of molybdates which can precipitate on cathodic and anodic sites in the alloy [46]. In particular, there is only one report in the literature evaluating the efficiency of cerium salts combined with molybdate in the corrosion inhibition of AZ91D alloy [13]. The authors describe the mechanism of coating formation and conclude that molybdate ions facilitate film deposition due to the strong oxidizing activity in the acid conversion solution.

It is known that the cerium coatings are principally composed by Ce^{3+} and Ce^{4+} with Ce^{4+} species as the main component. A superior anticorrosive performance in solutions containing chloride ions was obtained when a layer of Ce^{4+} oxide-hydroxides is formed. With respect to coloration, it has been reported that a coating rich in Ce^{4+} oxides gives from orange to dark yellow color while the pale yellow or translucent has been identified with larger amounts of Ce^{3+}species in the film [47,48]. In the present work the coating obtained in $Ce(NO_3)_3$ solution presented a grayish-white coloration while a dark yellow color was observed for the film electrodeposited

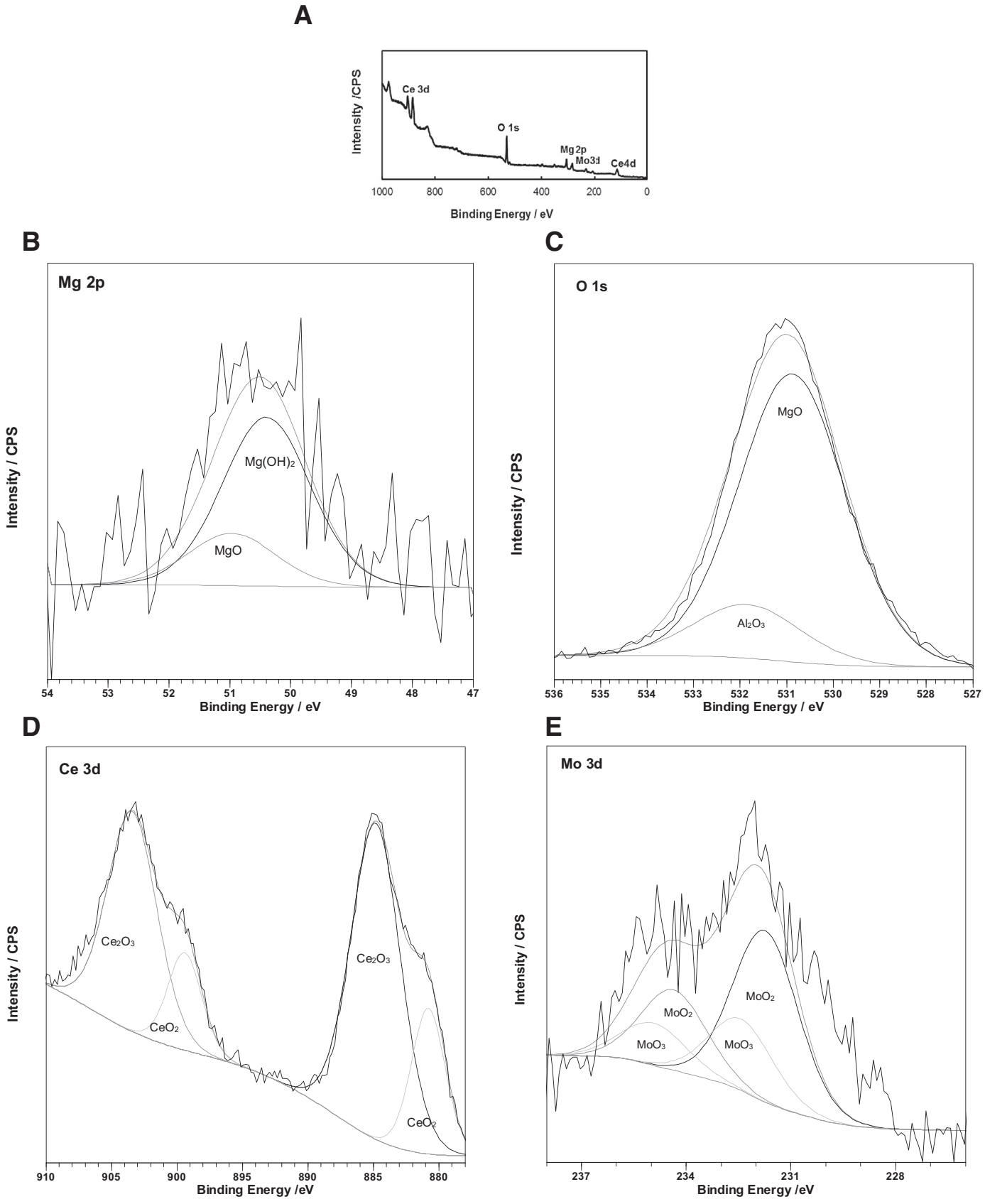

Fig. 11. (A) (A) XPS survey spectrum of Ce-Mo/H_3Cit-coat. XPS intensities of: (B) Mg 2p, (C) O 1s,(D) Ce 3d and (E) Mo 3d.

in the presence of $Ce(NO_3)_3$ and Na_2MoO_4. According to this, Ce^{4+} species are part of the film only when the treatment bath contains molybdate. Moreover, the presence of CeO_2 in the Ce-Mo/H_3Cit-coat was confirmed by XPS analysis. As was mentioned above, dissolved oxygen can promote the oxidation of Ce^{3+} to Ce^{4+} species. But in the light of the present results molybdate is the oxidizing agent, in accordance with the proposition of Du et al. [13], . From these results, we suggest that the yellow coloration is a consequence of the presence of molybdate in the treatment solution and its role as an oxidant.

With respect to the effects of H_3Cit it is known that a chelating agent should have two opposite effects on the corrosion of metals and may act as either an inhibitor or corrosive [49]. Wang informed that a cerium conversion coating on AZ91 magnesium alloy formed from ethanol solution containing $Ce(NO_3)_3$ and citric acid showed good corrosion performance [29]. The authors postulated that Mg ions originated from the dissolution of the alloy during immersion in the treatment bath reacted with Cit^{3-} and partly deposited on the alloy surface in form of Mg_3Cit_2 that is insoluble in ethanol. According to the theory of chemical adsorption of organic inhibitors, the chelating agent which forms a stable and insoluble chelate with a metal in certain medium can inhibit corrosion. Based on the results obtained here, we can propose that the formation of stable and insoluble chelates for H_3Cit concentration of 10 mM improves the corrosion resistance of AZ91D alloy. Moreover, the presence of H_3Cit as an additive leads to a closed structure and increases the adhesion of the deposited film.

As soon as the uncoated AZ91D alloy was immersed in Ringer solution, hydrogen bubbles evolution appeared. Then the surface was dissolved continuously. The corrosion starts at the interface of α and β phases owing to the micro-galvanic couple effect which plays an important role in accelerating the corrosion of the magnesium alloy) [25,49]. With the deposition of a stable cerium and molybdenum-based coating on magnesium alloy, the potential difference between α and β phases became small and the micro-galvanic couple effect was minimized.

According to the present results, the better anticorrosive performance is obtained by the formation of Ce-Mo/H_3Cit-coat. This improvement is associated with: (a) the presence of insoluble cerium oxides in the coating (b) the incorporation of molybdenum species in the film and (c) the formation of stable and insoluble chelates on the surface due the presence of H_3Cit in the electrodeposition solution.

4. Conclusions

An uniform, compact and adherent coating was obtained on AZ91D magnesium alloy in a solution containing $Ce(NO_3)_3$, Na_2MoO_4 and H_3Cit under potentiostatic conditions. The Ce-Mo/H_3Cit-coat is mainly composed by magnesium oxides or hydroxides and cerium and molybdenum oxides. A superior anticorrosive efficiency in simulated physiological solution was obtained with this film compared to those formed in the absence of H_3Cit. The improvement in the corrosion resistance is associated with the presence of insoluble precipitates of cerium and molybdenum oxides and the inhibiting properties of both molybdate and citric acid.

Acknowledgement

CONICET (PIP-112-201101-00055), ANPCYT (PICT-2015-0726) and Universidad Nacional del Sur (PGI 24/M127), Bahía Blanca, Argentina

References

[1] J.E. Gray, B. Luan, J. Alloys Comp. 336 (2002) 88–113.
[2] M. Khosro Aghayani, B. Niroumand, J. Alloys Comp. 509 (2011) 114–122.
[3] M. Staiger, A. Pietak, J. Huadmai, G. Dias, Biomaterials 27 (2006) 1728–1734.
[4] L. Weiping, Z. Liqun, L. Yihong, Surf. Coat. Technol. 201 (2006) 1085–1092.
[5] J. Sudagar, J. Lian, X. Chen, P. Lang, Y. Liang, Trans. Nonferrous Metal Soc. China 21 (2011) 921–928.
[6] Y. Zhang, C. Yan, F. Wang, H Lou, C. Cao, Surf. Coat. Technol. 161 (2002) 36–43.
[7] Y. Xu, X. Chen, Z. Lu, D. Zhou, L. Zhao, J. Harbin Inst. Technol. 6 (2001) 753–757.
[8] M.R. Elahi, M.H. Sohi, A. Safaei, Appl. Surf. Sci. 258 (2012) 5876–5880.
[9] L. Zhu, G. Song, Surf. Coat. Technol. 200 (2006) 2834–2840.
[10] T. Serikawa, M. Henmi, T. Yamaguchi, H. Oginuma, K. Kondoh, Surf. Coat. Technol. 200 (2006) 4233–4423.
[11] L. Anicai, R. Masi, M. Santamaria, F. Di Quarto, Corros. Sci. 47 (2005) 2883–2900.
[12] H. Hsiao, H. Tsung, W. Tsai, Surf. Coat. Technol. 199 (2005) 127–134.
[13] S. Mu, J. Du, H. Jiang, W. Li, Surf. Coat. Technol. 254 (2014) 364–370.
[14] J. Hu, Q. Li, X. Zhong, L. Zhang, B. Chen, Prog. Org. Coat. 66 (2009) 199–205.
[15] L. Pezzato, K. Brunelli, E. Napolitani, M. Magrini, M. Dabala, Appl. Surf. Sci. 357 (2015) 1031–1039.
[16] X. Li, S. Deng, H. Fu, Corros. Sci. 53 (2011) 2748–2753.
[17] R.W. Kapp Jr., Reference Module in Biomedical Sciences Encyclopedia of Toxicology, third ed. (2014).
[18] A.D. Forero Lopez, I.L. Lehr, S.B. Saidman, J. Alloys Compd. 702 (2017) 338–345.
[19] X.B. Chen, N. Birbilis, T.B. Abbott, Corrosion 67 (2011) 035005-1-035005-16.
[20] Z.Xu Y.Chen, C. Smith, J. Sankar, Acta Biomater 10 (2014) 4561–4573.
[21] S. Pommiers, J. Fryret, A. Castetbon, M. Potin-Gautier, Corros. Sci. 84 (2014) 135–146.
[22] H. Hornberger, S. Virtanen, A.R. Boccaccini, Acta Biomater 8 (2012) 2442–2455.
[23] X. Cui, Y. Yang, E. Liu, G. Jin, J. Zhong, Q. Li, Appl. Surf. Sci. 257 (2011) 9703–9709.
[24] M.F. Montemor, A.M. Simoes, M.G.S. Ferreira, M.J. Carmezim, Appl. Surf. Sci. 254 (2008) 1806–1814.
[25] J. Sun, G. Wang, Surf. Coat. Technol. 254 (2014) 42–48.
[26] A.P. Loperena, I.L. Lehr, S.B. Saidman, J. Magnesium Alloys 4 (2016) 278–285.
[27] A. Pardo, M. Merino, A. Coy, R. Arrabal, F. Viejo, E. Matykina, Corros. Sci. 50 (2008) 823–834.
[28] C. Wang, S. Zhu, F. Jiang, F. Wang, Corros. Sci. 51 (2009) 2916–2923.
[29] G. Song, A. Bowles, D. Stjohn, Mater. Sci. Eng. A 366 (2004) 74–86.
[30] T. Liu, S. Chen, S. Cheng, J. Tian, X. Chang, Y. Yin, Electrochim. Acta 52 (2007) 8003–8007.
[31] M. Mhaede, F. Pastorek, B. Hadzima, Mat. Sci. Engin. C 39 (2014) 330–335.

[32] M. Jamesh, S. Kumar, T.S.N. Sankara Narayanan, Corros. Sci. 53 (2011) 645–654.
[33] K. Brunelli, M Dabalá, J. Calliani, M. Magrini, Corros. Sci. 47 (2005) 989–1000.
[34] Y. Hamlaoui, F. Pedraza, C. Remazeilles, S. Cohendoz, C. Rébéré, L. Tifouti, J. Creus, Mater. Chem. Phys. 113 (2009) 650–657.
[35] Y.F. Zheng, X.N. Gu, F. Witte, Mater. Sci. Eng. R 77 (2014) 1–34.
[36] K.A. Yasakau, M.L. Zheludkevich, S.V. Lamaka, M.G.S. Ferreira, J. Phys. Chem. B 110 (2006) 5515–5528.
[37] C. Castano, M. O' Keefe, W. Fahrenholtz, Curr. Opin. Solid State Mater. Sci. 19 (2015) 69–76.
[38] L. Martínez, E. Román, J.L. de Segovia, S. Poupardb, J. Creus, F. Pedraza, App. Surf. Sci. 257 (2011) 6202–6207.
[39] I. Zhitomirsky, Adv. Colloid Interface Sci. 97 (2002) 279–317.
[40] A.J. Aldykiewicz Jr, A.J. Davenport, H.S. Isaacs, J. Electrochem. Soc. 143 (1996) 147–154.
[41] Y. Song, D. Shan, R. Chen, Surf. Coat. Technol. 204 (2010) 3182–3187.
[42] T. Ishizaki, Y. Masuda, K. Teshima, Surf. Coat. Technol. 217 (2013) 76–83.
[43] S.R. Taylor, B.D. Chambers, Corrosion 64 (2008) 255–270.
[44] M. Forsyth, T. Markley, D. Ho, G.B. Deacon, P. Junk, B. Hinton, A. Hughes, Corrosion 64 (2008) 191–197.
[45] C.B. Breslin, G. Treacy, W.M. Carroll, Corros. Sci. 36 (1994) 1143–1154.
[46] S.A. Hayes, P. Yu, T.J. O'Keefe, M.J. O'Keefe, J.O. Stoffer, J. Electrochem. Soc. 149 (2002) C623–C630.
[47] W.G. Fahrenholtz, M.J. O'Keefe, H. Zhou, J.T. Grant, Surf. Coat.Technol. 155 (2002) 227.
[48] M. Katoh, Corros. Sci 8 (1968) 423–431.
[49] Y.W. Song, D.Y. Shan, E.H. Han, Electrochim. Acta. 53 (2008) 2135–2143.